RSC Advances

PAPER

View Article Online
View Journal | View Issue



Cite this: *RSC Adv.*, 2026, **16**, 28592

# Cytocompatible and photoluminescent nitrogen-doped carbon dots derived from grape seed flour for enhanced fluorescence bioimaging in breast cancer cells

Fatmanur Uyumaz Cengiz, [a] Ayşegül Açıksarı,[b] Ramazan Ceylan,[bc] Sibel Çetinel, [bc] Gökhan Kafes,[d] Özgül Gök, [d] Ayşe Dulda [e] and Memet Vezir Kahraman *[a]

Carbon dots (CDs) have attracted significant attention as fluorescent nanomaterials due to their tunable optical properties, low toxicity, and versatile surface chemistry. However, the development of sustainable and cost-effective synthesis routes remains an ongoing challenge. In this study, nitrogen-doped carbon dots (N-CDs) were synthesized *via* a simple and green solid-state method using grape seed flour as a renewable carbon source, together with citric acid and urea. The obtained N-CDs exhibited bright green photoluminescence with an emission maximum at 539 nm, a high quantum yield of 62.6%, and a large Stokes shift (~89 nm). Structural and surface analyses (FTIR, XRD, STEM, and XPS) confirmed the formation of well-dispersed, nearly spherical nanoparticles (9–18 nm) with abundant oxygen- and nitrogen-containing functional groups. These surface functionalities contributed to excellent aqueous dispersibility and colloidal stability. *In vitro* cytotoxicity studies demonstrated that the N-CDs maintained high cell viability (>70%) in MCF-7 and SK-BR-3 cells up to 400 μg $mL^{-1}$, indicating good biocompatibility. Confocal microscopy revealed efficient cellular uptake, which was further enhanced after folic acid conjugation, suggesting receptor-mediated internalization. Overall, this work presents a sustainable approach for producing biocompatible, highly luminescent carbon dots from biomass resources and highlights their potential as fluorescent probes for bioimaging applications.

Received 22nd March 2026
Accepted 20th May 2026

DOI: 10.1039/d6ra02360f

rsc.li/rsc-advances



## 1. Introduction

Carbon-based nanoparticles, widely known as carbon dots (C-dots), have emerged as a versatile and rapidly expanding class of nanomaterials with substantial potential in nanomedicine. Typically below 10 nm in diameter, C-dots display remarkable photophysical features, including strong and tunable photoluminescence, excellent photostability, and high aqueous dispersibility.[1–4] These attributes, together with their intrinsic biocompatibility and negligible cytotoxicity, make them highly attractive for applications such as fluorescence imaging, biosensing, and drug delivery.

A variety of synthetic strategies, including hydrothermal carbonization, microwave-assisted synthesis, and pyrolytic conversion of carbon-rich precursors, allow precise control over size distribution, crystallinity, and surface chemistry.[5–7] Post-synthetic surface passivation or heteroatom doping can further enhance solubility, colloidal stability, and biological specificity.[8–10] As a result, functionalized C-dots have been widely investigated as targeted fluorescent probes and nanocarriers in cancer theranostics, where simultaneous imaging and therapy are desired.[11,12]

In parallel with advances in synthesis, considerable interest has shifted toward green and sustainable routes for C-dot production. Biomass-derived C-dots, prepared from renewable resources such as fruit peels, vegetable residues, and agricultural by-products, offer a cost-effective and environmentally benign alternative while minimizing toxicity—an essential factor for biomedical use.[13,14] Black grape seed flour is a particularly promising precursor, as its high polyphenolic content imparts strong antioxidant activity and bright photoluminescence to the resulting C-dots, thereby enhancing their suitability for bioimaging and therapeutic applications.[15–17]

[a]*Department of Chemistry, Faculty of Science, Marmara University, Istanbul, Turkiye. E-mail: mvezir@marmara.edu.tr*
[b]*Nanotechnology Research and Application Center (SUNUM), Sabanci University, Istanbul, Turkiye*
[c]*Faculty of Engineering and Natural Sciences, Sabanci University, Istanbul, Turkiye*
[d]*Department of Biomedical Engineering, Graduate School of Natural and Applied Sciences, Acibadem Mehmet Ali Aydinlar University, Istanbul, Turkiye*
[e]*Department of Mechatronics Engineering, Faculty of Engineering and Architecture, Istanbul Nisantasi University, Istanbul, Turkiye*

The biomedical relevance of these nanoplatforms is underscored by their potential in breast cancer research. Breast cancer remains one of the most prevalent malignancies and a leading cause of cancer-related mortality among women globally.[18] Its pathogenesis involves uncontrolled proliferation of mammary epithelial cells, tumor progression, and eventual metastasis. Based on molecular profiles, breast cancers are classified into distinct subtypes with differing prognoses and therapeutic responses. For instance, MCF-7 cells express estrogen receptors and are responsive to endocrine therapy,[19,20] whereas SK-BR-3 cells are HER2-positive breast cancer cells characterized by HER2 overexpression, making them an important model for targeted cancer imaging and therapeutic studies.[20,21] Understanding these subtype-specific differences is critical for designing effective and personalized therapeutic strategies.

Recent trends in nanomedicine emphasize the development of strategies that selectively target cancer cells, inhibit proliferation, and induce apoptosis, thereby maximizing therapeutic efficacy while minimizing systemic toxicity.[22,23] C-dots provide a flexible platform for such approaches: conjugation with folic acid enables binding to folate receptors frequently overexpressed on breast cancer cells, whereas RGD-based peptides facilitate integrin-mediated internalization and enhance cellular uptake.[24,25] These functional modifications improve tumor selectivity, intracellular accumulation, and therapeutic outcomes while minimizing off-target effects.

Recent advances in carbon-dot research have focused on improving photoluminescence efficiency, tunable emission behavior, and biomedical applicability through heteroatom doping, surface engineering, and sustainable synthesis strategies. In addition, emerging approaches including machine learning-assisted synthesis and structure–property optimization have further accelerated the development of high-performance fluorescent carbon nanomaterials for sensing and bioimaging applications.[26–29]

Although numerous biomass-derived carbon dots have been reported, many previously described synthesis approaches rely on hydrothermal or solvent-assisted methods that require relatively long reaction times, complex purification steps, or produce carbon dots with limited fluorescence efficiency. In addition, reports on grape seed flour-derived carbon dots with strong green fluorescence emission and high quantum yield remain limited. In this context, the present study introduces a simple and sustainable solid-state synthesis strategy for producing nitrogen-doped carbon dots from grape seed flour without the need for additional solvent-based reaction systems. The synthesized N-CDs exhibit relatively high quantum yield, stable fluorescence behavior, favorable cytocompatibility, and efficient cellular imaging performance, demonstrating their potential as environmentally friendly fluorescent nanomaterials for bioimaging applications. Black grape seed flour was selected as a sustainable biomass precursor owing to its abundance, low cost, and rich chemical composition, including polyphenolic compounds, aromatic structures, carbohydrates, and oxygen-containing functional groups. These constituents can contribute to carbon core formation during thermal carbonization and provide surface-active sites that improve aqueous dispersibility and photoluminescence behavior. Compared with conventional molecular precursors alone, the use of grape seed flour introduces a renewable and naturally functionalized carbon source, supporting the development of environmentally friendly N-CDs for biomedical applications.

This study aims to synthesize carbon dots from black grape seed flour, functionalize them with targeting ligands such as folic acid, and systematically evaluate their uptake and imaging performance in breast cancer cell models (MCF-7 and SKBR-3). The overarching goal is to demonstrate the potential of sustainably derived C-dots as multifunctional nanoplatforms for simultaneous cancer detection and therapeutic intervention.

## 2. Experimental

### 2.1 Materials

Grape seed flour was purchased from a local market (Turkiye). Citric acid and urea were purchased from Sigma Aldrich, Netherlands.

### 2.2 Synthesis of nitrogen-doped carbon dots (N-CDs)

Nitrogen-doped carbon dots (N-CDs) were synthesized *via* a solid-state carbonization approach (Fig. 1). Briefly, 0.75 g black grape seed flour, 0.25 g citric acid, and 1.0 g urea were thoroughly ground using a mortar and pestle until a homogeneous fine powder was obtained. The mixture was transferred into a 100 mL heat-resistant beaker and subjected to thermal carbonization in a laboratory oven at 200 °C for 1 h. Following natural cooling to ambient temperature, the carbonized material was dispersed in 30 mL of ultrapure water and homogenized using ultrasonication for 30 min to facilitate particle disintegration and uniform dispersion. The resulting suspension was centrifuged at 12 000 rpm for 20 min to remove large aggregates, and the supernatant was carefully collected. To further eliminate residual particulates, the supernatant was passed through a 0.22 μm syringe filter. For purification, the filtrate was dialyzed against ultrapure water for 48 h using a dialysis membrane with a molecular weight cut-off of 1000 Da, with frequent water replacement to ensure removal of unreacted precursors and small molecular impurities. The purified N-CD solution was subsequently freeze-dried to obtain a dry powder, which was re-dispersed in phosphate-buffered saline (PBS, pH 7.0) at a final concentration of 2 mg $mL^{-1}$ for downstream characterization and biological assays.

The reaction temperature and time were selected based on preliminary optimization experiments and previously reported thermal carbonization conditions for biomass-derived and citric acid/urea-based carbon dots. Lower temperatures or shorter reaction times produced weakly fluorescent products, suggesting insufficient carbonization, whereas excessive heating led to over-carbonized materials with reduced water dispersibility. Therefore, carbonization at 200 °C for 1 h was chosen as a balanced condition that enables N-CD formation while retaining oxygen- and nitrogen-containing surface functionalities. The successful formation of N-CDs under these conditions

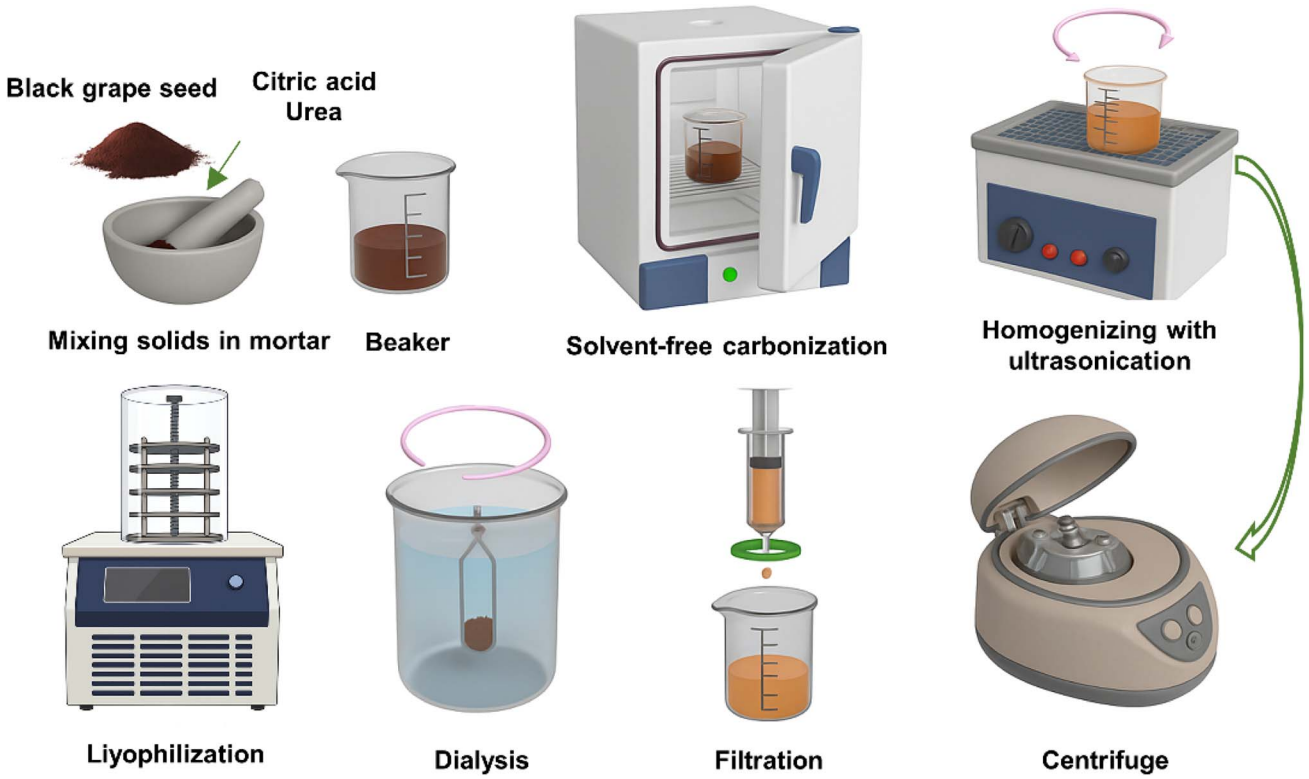


Fig. 1 Synthesis scheme of N-CDs.

was confirmed by the obtained optical, morphological, and chemical characterization results.

### 2.3 Characterization of N-CDs

The structural, optical, and chemical properties of the synthesized N-CDs were characterized using a combination of spectroscopic and microscopic techniques. Fourier-transform infrared spectroscopy (FTIR, PerkinElmer Spectrum 100, USA) was performed in the 4000–400 $cm^{-1}$ range to identify functional groups. UV–Vis absorption spectra were recorded on a Shimadzu UV-2450 spectrophotometer to examine electronic transitions, while photoluminescence (PL) spectra were measured under ambient conditions using a Hitachi F-7000 spectrofluorometer with 1 cm quartz cuvettes.

Crystallinity and phase information were obtained by X-ray diffraction (XRD) using a Philips diffractometer with Cu Kα radiation ($\lambda$ = 1.5406 Å). Surface morphology and internal structures were analyzed using scanning electron microscopy (SEM) and scanning transmission electron microscopy (STEM) (Thermo Scientific Quattro S). X-ray photoelectron spectroscopy (XPS, Thermo Fisher Scientific K-Alpha) was used to determine the elemental composition and chemical states of the surface.

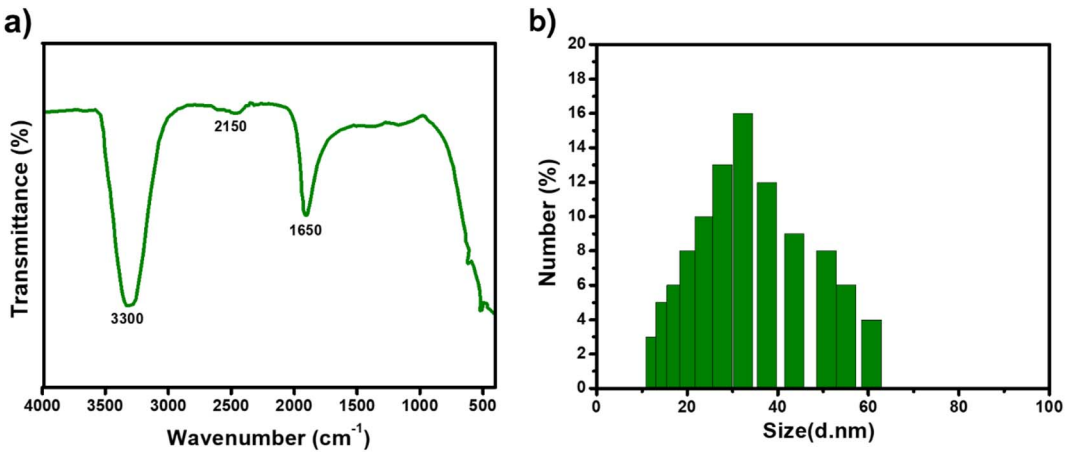


Fig. 2 (a) FTIR spectrum and (b) DLS measurement of N-CDs.

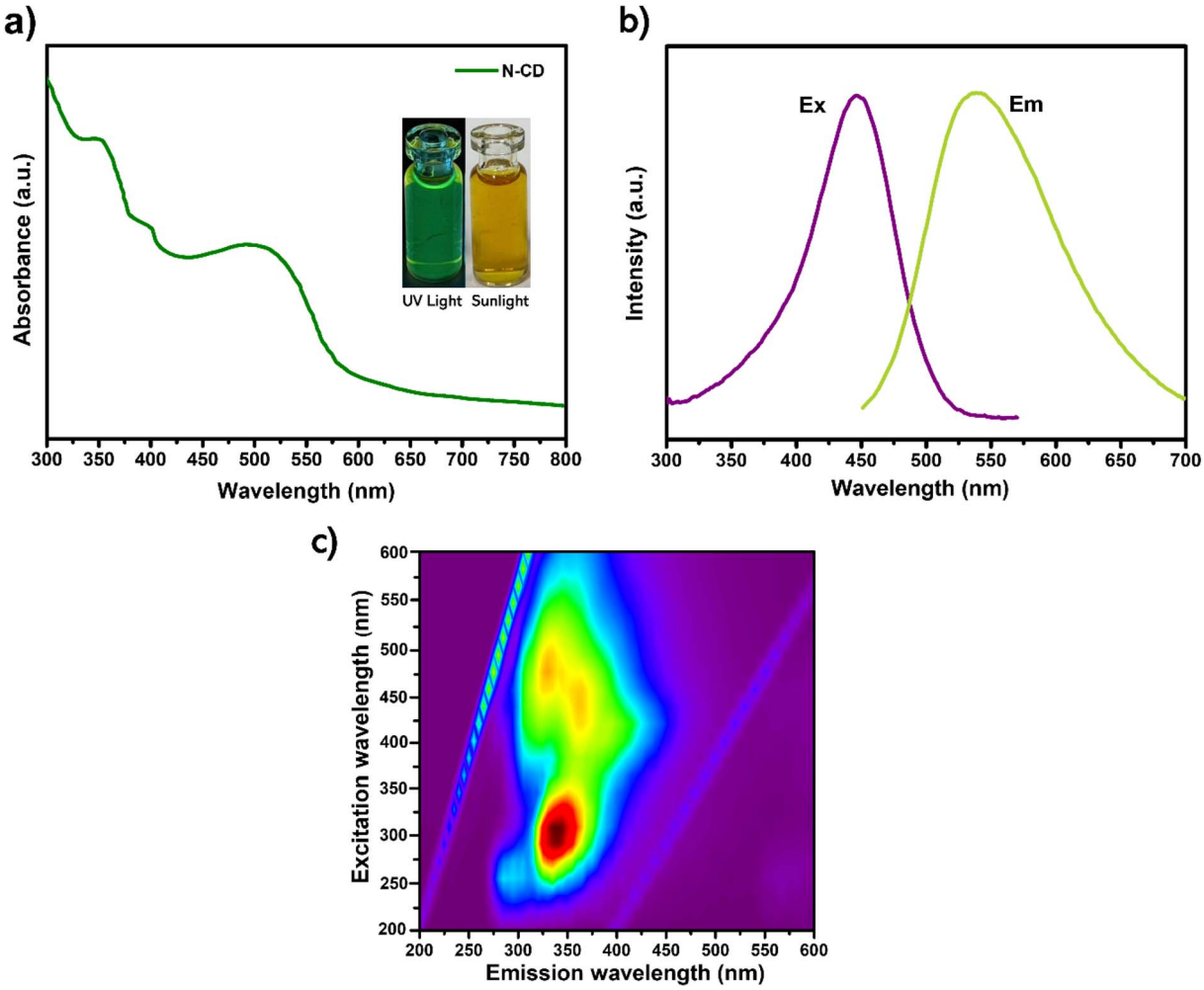


Fig. 3 Optical properties of N-CDs: (a) UV–Vis spectrum and digital images under UV light and sunlight, (b) PL excitation and emission spectra showing green fluorescence (c) 3D PL map of CQDs.

The photoluminescence quantum yield (PL QY) was measured by a relative method using Rhodamine B ($\varphi = 0.71$ in ethanol, $\lambda_{ex} = 450$ nm) as the reference. The QY was calculated using:

$$\varphi_{CD} = \varphi_{RhB} \times \left(\frac{I_{CD}}{I_{RhB}}\right) \times \left(\frac{\eta_{CD^2}}{\eta_{RhB^2}}\right)$$

where $I$ is the integrated emission intensity and $\eta$ is the solvent refractive index. Since both sample and reference were measured at low absorbance values ($A < 0.1$) to minimize inner filter effects, no absorbance correction factor was required. When both sample and reference were measured in solvents with identical or very similar refractive indices (*e.g.*, water: $n = 1.33$; ethanol: $n = 1.36$), the correction factor involving $\eta\backslash eta\eta$ was considered negligible.

The environmental stability of the N-CDs was evaluated by monitoring the photoluminescence intensity under different pH, temperature, and ionic conditions. For pH stability, the pH of aqueous N-CD dispersions was adjusted between 3 and 11 using dilute HCl or NaOH solutions. Thermal stability measurements were performed after incubating the dispersions at different temperatures (25–100 °C). Ionic stability was investigated in the presence of various salt solutions (10 mM). The fluorescence emission intensity was recorded at $\lambda_{em} = 539$ nm under 450 nm excitation.

### 2.4 *In vitro* analysis

MCF-7 (human breast adenocarcinoma) and SK-BR-3 (HER2-positive breast cancer) cells were obtained from American type culture collection (ATCC). Cells were grown at 37 °C in a humid environment with 5% $CO_2$ in Dulbecco's Modified Eagle Medium (DMEM, high glucose) with 10% fetal bovine serum (FBS) and 1% penicillin-streptomycin (100 U $mL^{-1}$ penicillin and 100 μg $mL^{-1}$ streptomycin). Both cell lines were subcultured to around 70–80% confluence. Cells were washed with phosphate-buffered saline (PBS), detached with 0.05% trypsin–EDTA, and reseeded at the appropriate density (1 : 4 to 1 : 6). Medium was changed every 2–3 days.

**2.4.1 Cytotoxicity experiments.** The cytotoxicity of manufactured N-CDs was determined in MCF-7 and SK-BR-3 cell lines using the Cell Counting Kit-8 (CCK-8, MedChemExpress, NJ,

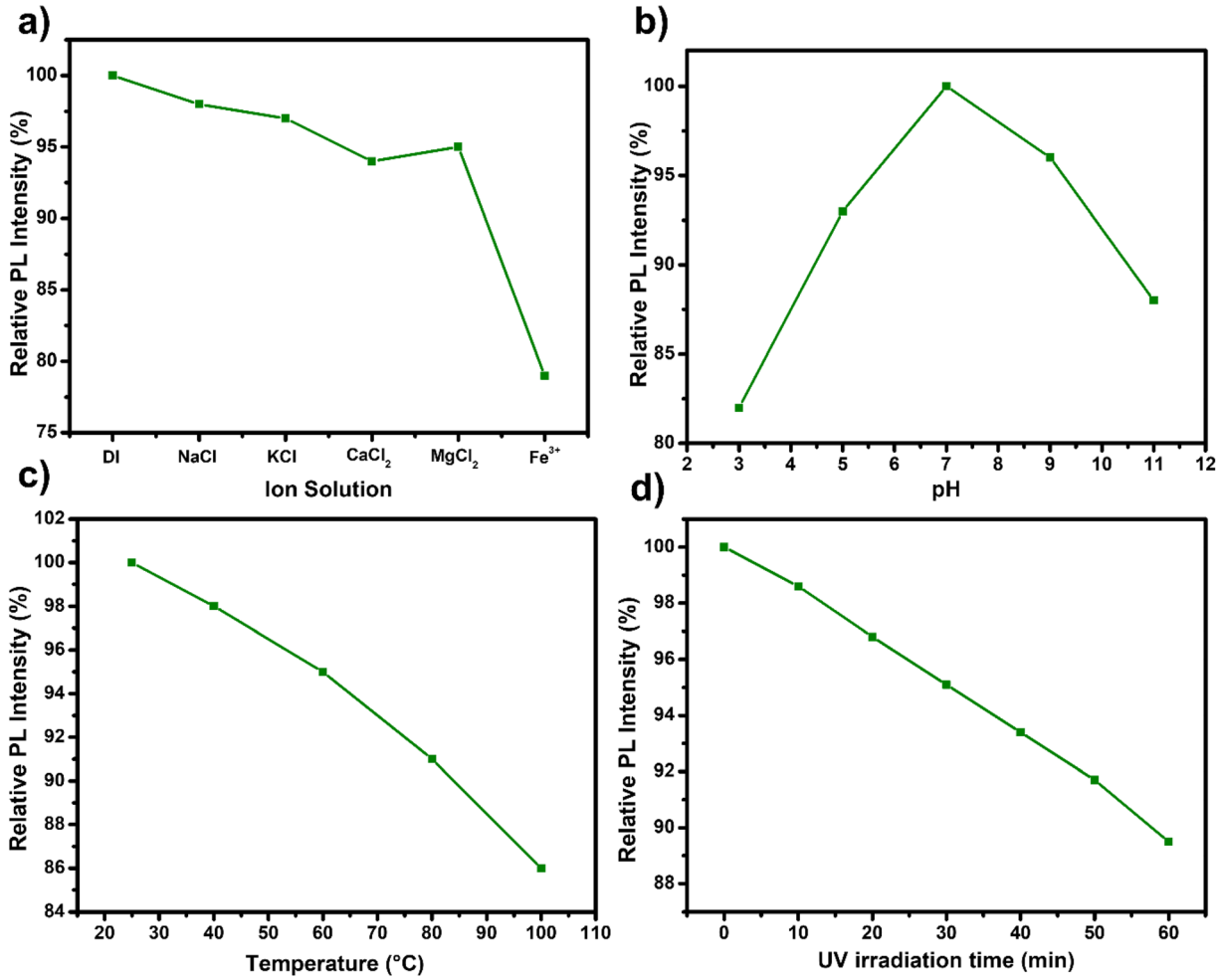


Fig. 4 Stability evaluation of the synthesized N-CDs: (a) relative PL intensity in different ionic solutions, (b) PL behavior under various pH conditions, (c) fluorescence stability at different temperatures, and (d) photostability under continuous UV irradiation.

USA) assay. Cells were seeded in 96-well plates at a density of $1 \times 10^4$ cells per well in 100 μL of complete media, then incubated for 24 hours at 37 °C in a humidified 5% $CO_2$ environment.

After incubation, cells were treated with N-CDs suspensions at different concentrations (50, 100, 200, and 400 μg $mL^{-1}$) in culture media. After 24 hours of exposure, 10 μL of CCK-8 reagent was added to each well, and the plates were incubated for further 2 hours at 37 °C. The absorbance of each well was measured at 450 nm using a microplate reader (TECAN). Cell viability was represented as a proportion of the control group (untreated cells). All experiments were performed at least three times.

**2.4.2 Cellular uptake of the particles.** To evaluate the cellular uptake of N-CDs, MCF-7 and SK-BR-3 cells were seeded onto sterilized glass coverslips in 12-well plates at a density of $2 \times 10^5$ cells per well and incubated overnight. The cells were treated with 100 μg $mL^{-1}$ N-CDs diluted in complete culture media for 4 and 24 hours. After incubation, cells were washed three times with PBS to eliminate any excess nanoparticles. The cells were then fixed in 4% paraformaldehyde for 15 minutes at room temperature. Coverslips were put on glass slides with DAPI mounting medium. A confocal laser scanning microscope (Carl Zeiss 710 LSM confocal microscope) was used to observe cellular internalization and intracellular distribution of N-CDs. N-CDs were excited at the appropriate laser line (488 nm). Images were processed and examined with microscope software (Zeiss Zen 3.9).

## 3. Results and discussion

The FTIR spectrum of the synthesized N-CDs (Fig. 2a) confirms the presence of multiple surface functional groups derived from the precursor materials. A broad band around ~3300 $cm^{-1}$ is assigned to the stretching vibrations of hydroxyl (–OH) and/or amine (–NH) groups, originating primarily from citric acid and urea.[30] This broad feature also indicates the presence of physically adsorbed water, consistent with the hydrophilic surface characteristics of carbon dots. A weaker band near ~2150 $cm^{-1}$ can be attributed to C≡C (alkyne) or C≡N (nitrile) stretching vibrations, commonly observed in nitrogen-doped carbon nanostructures and likely formed during the thermal decomposition of nitrogen-containing precursors such as

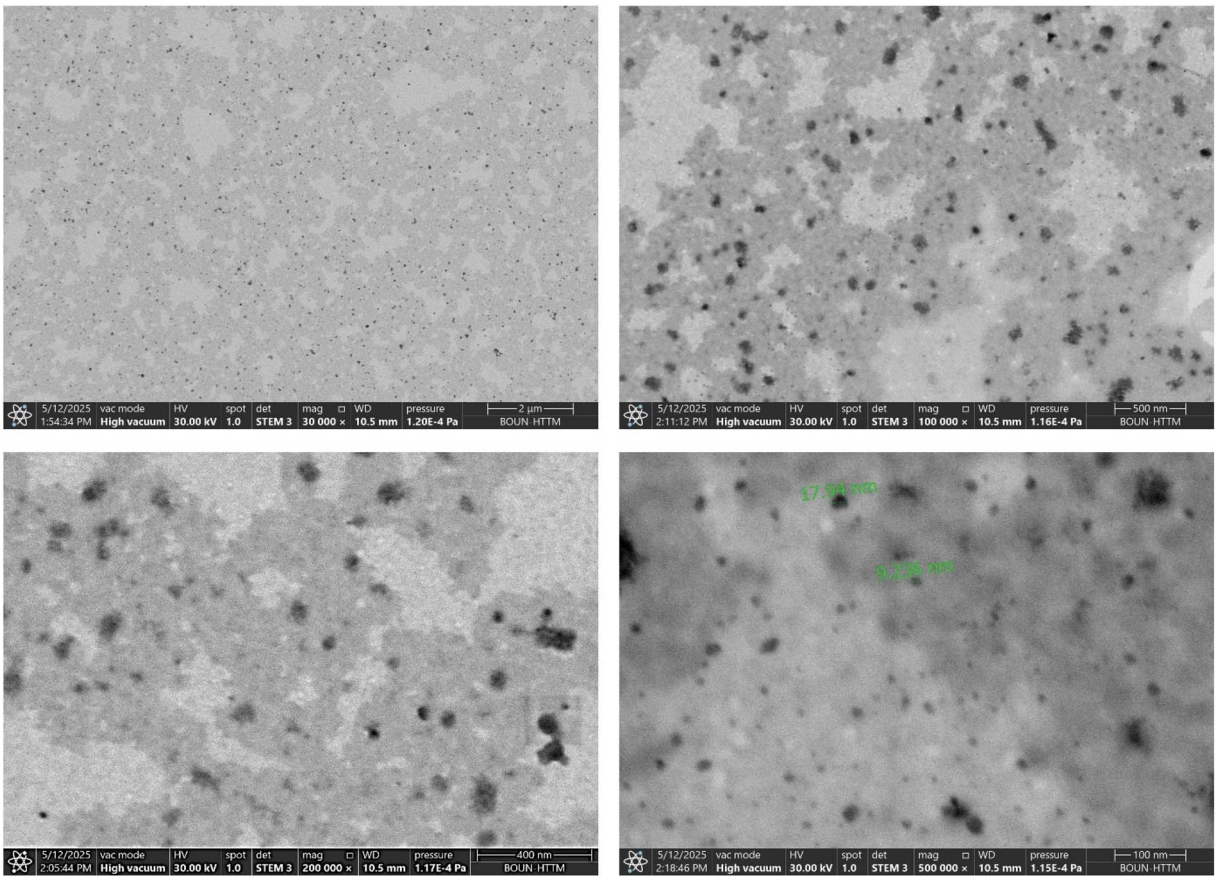


Fig. 5 STEM images of N-CDs at varying magnifications.

urea.[31] A pronounced absorption peak at ~1650 $cm^{-1}$ corresponds to C=O stretching vibrations, which may arise from carbonyl functionalities (carboxylic acids, amides, or esters) generated during the carbonization of citric acid.[32] Collectively, these spectral features confirm that the N-CDs are enriched with oxygen- and nitrogen-containing functional groups. Such surface moieties not only enhance aqueous dispersibility but also provide accessible reactive sites for subsequent functionalization, thereby increasing the suitability of these nanomaterials for optoelectronic, sensing, and biomedical applications.

Dynamic light scattering (DLS) measurements (Fig. 2b) were conducted to determine the hydrodynamic size distribution of the N-CDs in aqueous suspension. The resulting histogram revealed that most particles were distributed within the 10–60 nm range, with a predominant peak centered around 30–35 nm. The relatively narrow distribution indicates a near-monodisperse population and suggests limited aggregation, likely due to electrostatic stabilization and steric hindrance imparted by surface functional groups. It is important to note that DLS determines the hydrodynamic diameter, which accounts for both the carbon core and its associated solvation layer. Consequently, the actual core diameter of the N-CDs is expected to be smaller, typically within 5–15 nm, as commonly observed in high-resolution imaging techniques such as STEM.[33]

The UV–Vis absorption spectrum (Fig. 3a) of the N-CDs exhibits a prominent band at ~350 nm, typically assigned to n–π* transitions of conjugated carbonyl (C=O) and imine (C=N) groups.[34,35] A secondary, well-defined absorption feature is observed at ~485 nm.[36] Three-dimensional photoluminescence spectra show that excitation at 450 nm produces a strong emission maximum at ~539 nm (Fig. 3c). The overlap between the emission profile and the 485 nm absorption band indicates that the green fluorescence arises predominantly from this transition rather than the 350 nm band, suggesting that UV excitation does not contribute significantly to green emission (Fig. 3b). Furthermore, the 3D PL map reveals partially excitation-dependent fluorescence behavior with multiple emissive regions at different excitation wavelengths. Such behavior is commonly associated with heterogeneous surface states, different emissive trapping sites, and variations in the size/surface chemistry of carbon-dot domains, which are frequently observed in biomass-derived carbon nanomaterials.

The photoluminescence quantum yield (PL QY) of the N-CDs was measured as 62.6% using rhodamine B as the reference fluorophore. The observed emission corresponds to a Stokes shift of ~89 nm (539 – 450 nm), indicative of efficient relaxation processes prior to radiative recombination. The relatively high

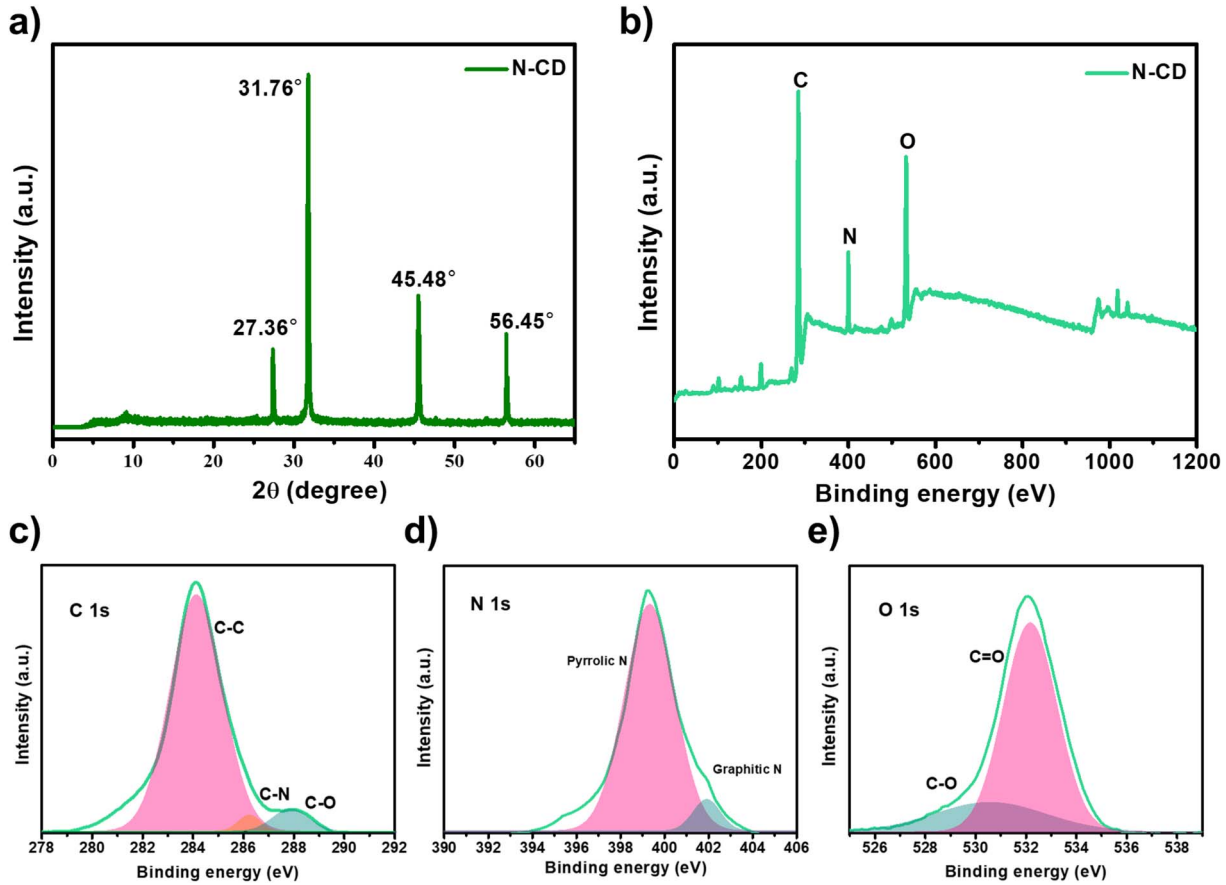


Fig. 6 (a) XRD pattern, (b) XPS survey spectrum, (c) high-resolution C 1s spectrum, (d) high-resolution N 1s spectrum, (e) high-resolution O 1s spectrum of N-CDs.

quantum yield of the synthesized N-CDs can likely be attributed to the combined effects of nitrogen doping and effective surface passivation. Nitrogen-containing functional groups introduced from urea may create additional emissive surface states and modify the electronic structure of the carbon framework, thereby enhancing radiative recombination processes. In addition, abundant oxygen- and nitrogen-containing surface functionalities can reduce surface defects that typically act as non-radiative recombination centers. The partially ordered graphitic domains suggested by XRD may additionally contribute to enhanced electronic delocalization and improved fluorescence efficiency. Collectively, these factors are believed to be responsible for the enhanced photoluminescence performance and relatively high quantum yield of the N-CDs.

The stability of the N-CDs was further investigated under different ionic, pH, temperature, and UV irradiation conditions (Fig. 4). The N-CDs maintained stable fluorescence emission over a broad pH range, with only moderate decreases under strongly acidic or alkaline conditions, indicating relatively stable emissive surface states. Similarly, the PL intensity was largely preserved at elevated temperatures, demonstrating good thermal stability of the carbon framework. In ionic media, most common salt solutions resulted in only minor variations in fluorescence intensity, whereas $Fe^{3+}$ ions induced noticeable fluorescence quenching, likely due to electron- or energy–transfer interactions with surface functional groups. In addition, the N-CDs retained most of their initial fluorescence intensity after continuous UV irradiation, demonstrating favorable photostability of the emissive system. These findings collectively demonstrate the favorable environmental and photochemical stability of the synthesized N-CDs and support their potential applicability in bioimaging-related applications.

STEM analysis (Fig. 5) reveals a uniform distribution of well-dispersed, nearly spherical N-CDs. At 30 000× magnification, the sample appears as a continuous, homogeneous matrix with no visible agglomeration. At higher magnifications (100 000×–500 000×), individual nanoparticles are clearly resolved, exhibiting consistent morphology and sharp contrast. Direct size measurements indicate particle diameters of approximately 9–18 nm, confirming a narrow size distribution. Similar studies have reported well-dispersed, spherical carbon dots with particle sizes in the range of 10–20 nm.[37,38]

The absence of clustering and the high degree of dispersion suggest effective surface passivation by oxygen and nitrogen-containing functional groups originating from citric acid and urea precursors. This passivation likely contributes to colloidal stability by preventing aggregation through electrostatic and steric effects.[39] Collectively, these results confirm the successful

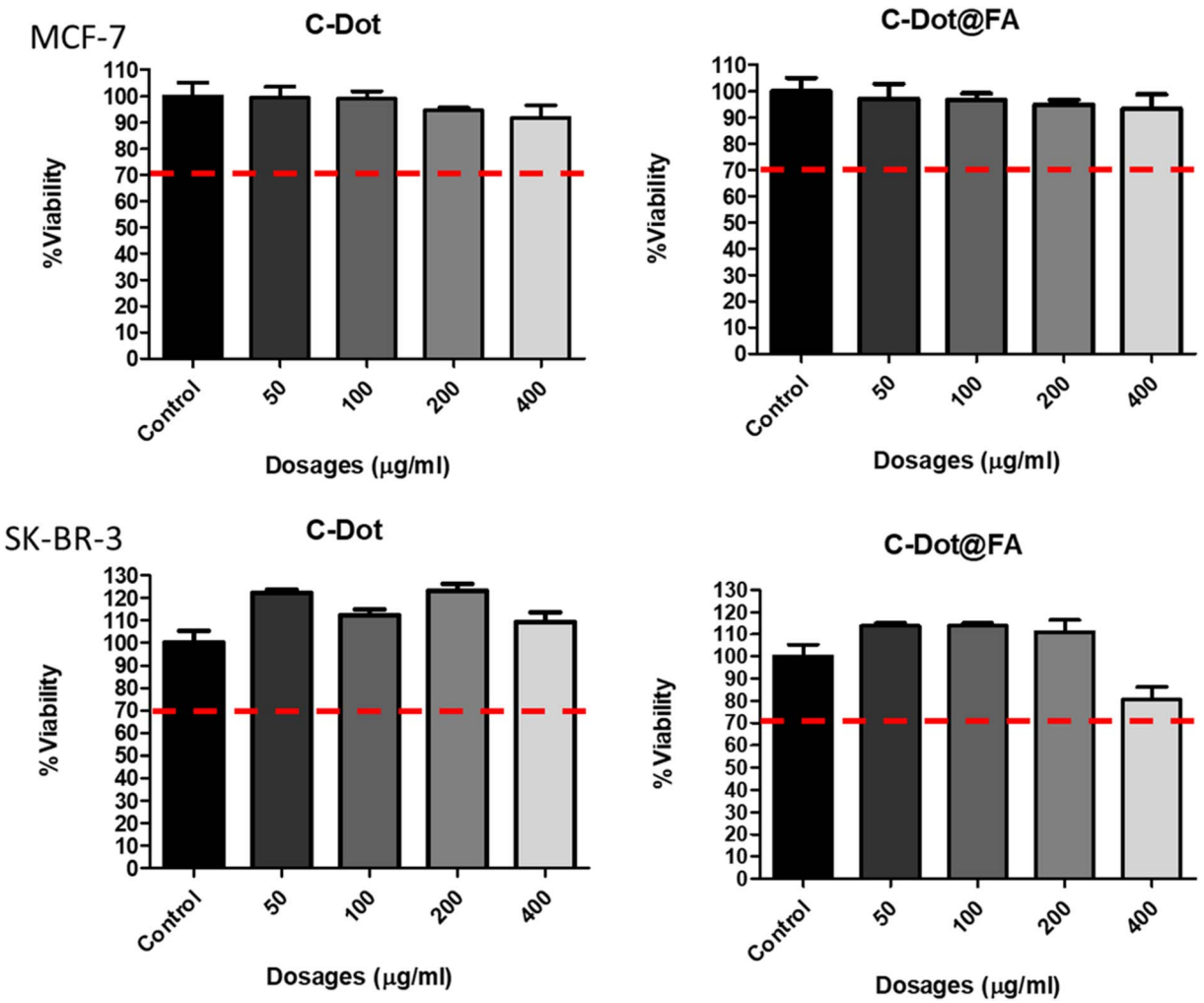


Fig. 7 Cytotoxicity of C-dot and C-dot-FA nanoparticles in MCF-7 and SK-BR-3 cells. Cell viability was assessed after treatment with nanoparticles at concentrations ranging from 50 to 400 μg $mL^{-1}$.

synthesis of nanoscale carbon dots with desirable morphological uniformity for biomedical and optoelectronic applications.

The XRD pattern of the synthesized N-CDs (Fig. 6a) exhibits broad and weak diffraction features, indicating the predominantly amorphous nature of the carbon framework together with partially ordered graphitic domains. Such diffraction behavior is commonly observed in biomass-derived carbon dots due to incomplete graphitization and the presence of heterogeneous surface functionalities. In addition, some diffraction signals may also originate from residual inorganic/mineral components naturally present in the biomass precursor. Overall, the XRD results support the formation of partially carbonized nanoscale structures rather than highly crystalline graphitic carbon.[40,41]

The XPS survey spectrum (Fig. 6b) further validates the elemental composition of the N-CDs, showing pronounced peaks corresponding to C 1s (~284 eV), N 1s (~400 eV), and O 1s (~532 eV), confirming the successful incorporation of nitrogen and oxygen species into the carbon framework.[42]

High-resolution deconvolution of the C 1s spectrum (Fig. 6c) reveals three components assigned to C–C/C=C (~284.5 eV), C–N (~285.8 eV), and C–O (~287.1 eV), reflecting the coexistence of graphitic carbon and heteroatom-functionalized groups.[43,44] The N 1s spectrum (Fig. 6d) shows two primary peaks at ~399.8 eV and ~401.2 eV, corresponding to pyrrolic N and graphitic N, respectively, an indication of successful nitrogen doping, which is known to enhance electronic conductivity and active site density.[44,45] The O 1s spectrum (Fig. 6e) is deconvoluted into two peaks assigned to C=O (~531.6 eV) and C–O (~533.1 eV) groups, which contribute to hydrophilicity and colloidal stability in aqueous media.[46]

The cytotoxicity of N-CDs should be considered because they have the potential to be used in bio-imaging due to their superior fluorescence stability. To assess the cytotoxicity of C-dot and C-dot-FA, the CCK-8 method was used to evaluate the viability of MCF-7 and SK-BR-3 cells treated with the C-dots. Across the tested concentration range of 50–400 μg $mL^{-1}$, cell viability remained above 70% in both cell lines, indicating no significant toxic effects of the nanoparticles (Fig. 7).

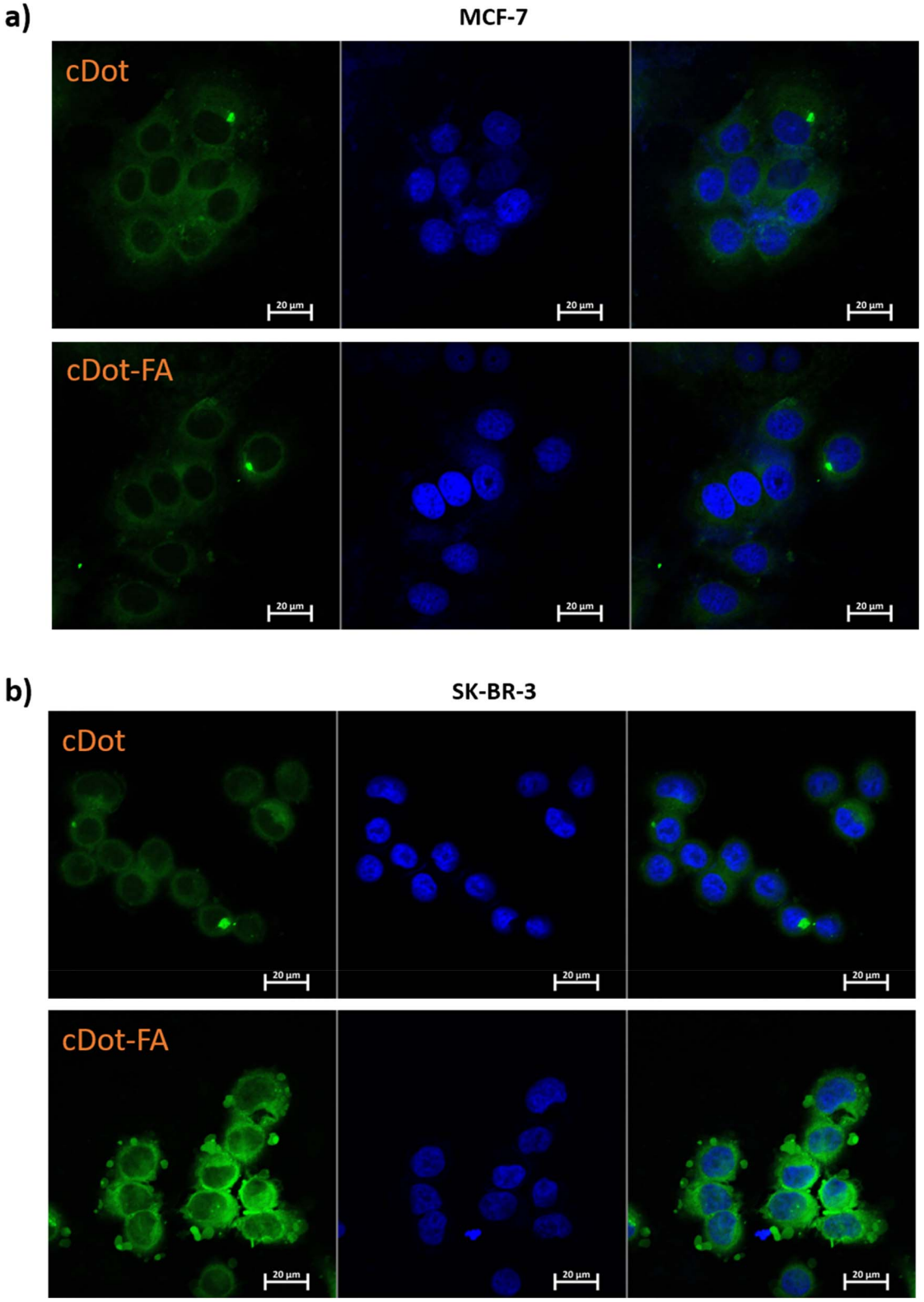


Fig. 8 Confocal microscopy images showing internalization of C-dot and C-dot-FA nanoparticles in MCF-7 (a) and SK-BR-3 cells (b) after 4 hours of incubation.

To analyze the possible use of N-CDs in cell imaging *in vitro*, MCF-7 and SK-BR-3 cells were treated with C-dot and C-dot-FA solutions for 4 h. MCF-7 and SK-BR-3 cell uptake of C-dot and C-dot-FA was displayed *via* laser scanning confocal microscopy (Fig. 8a and b). In MCF-7 cells, both nanoparticles had comparable fluorescence. However, in the case of SK-BR-3 cells,

Table 1 Comparison of the synthesized N-CDs with previously reported biomass-derived carbon dots for bioimaging applications

| Carbon source | Synthesis method | Emission | QY (%) | Bioimaging | Ref. |
|---|---|---|---|---|---|
| Rapeseed pollen | Hydrothermal | Blue | 7.7 | Yes | 51 |
| Milk | Hydrothermal | Blue | 12 | Yes | 15 |
| Tapioca | Hydrothermal | Blue-green | 34.9 | Limited | 30 |
| Grape seed | Hydrothermal | Blue | — | Not reported | 16 |
| This work (grape seed flour) | Solid-state | Green | 62.6 | Yes | This work |

C-dot-FA produced noticeably stronger fluorescence signals than C-dot. Accordingly, these findings are consistent with the folate receptor mediated endocytosis mechanism.[47,48] Folic acid increases the uptake of nanoparticles by the cells *via* folate receptor's binding (especially FR$\alpha$) on the cell surface.[48,49] Also, previous research show that folate receptor–targeted nanoparticles can be efficiently internalized in SK-BR-3 cells.[50] According to this, receptor-mediated mechanisms facilitates the uptake behavior. These results support our finding that C-dot-FA increased fluorescence, indicating that FA conjugation promotes cellular entrance in this cell line.

A comparison with previously reported biomass-derived carbon dots is summarized in Table 1. Compared with many previously reported systems, the synthesized N-CDs exhibit relatively high quantum yield together with stable green fluorescence emission and good cytocompatibility. In addition, the present study utilizes a simple and sustainable solid-state synthesis strategy using grape seed flour as a renewable precursor, without requiring complex solvent-assisted procedures. These combined characteristics demonstrate the potential of the synthesized N-CDs as environmentally friendly fluorescent nanomaterials for bioimaging-related applications.

## 4. Conclusion

In this study, nitrogen-doped carbon dots (N-CDs) were synthesized from grape seed flour *via* a simple and sustainable solid-state route. Comprehensive characterization confirmed well-dispersed, nearly spherical nanoparticles (~9–18 nm) with a predominantly amorphous carbon framework with partially ordered graphitic domains and abundant nitrogen/oxygen surface functionalities, which enhance hydrophilicity and provide sites for further functionalization. The N-CDs exhibited bright green photoluminescence ($\lambda_{em} \approx 539$ nm) with a high quantum yield (62.6%) and a large Stokes shift (~89 nm), making them excellent candidates for bioimaging applications. *In vitro* studies demonstrated high cytocompatibility (>70% cell viability up to 400 μg mL$^{-1}$) and efficient cellular uptake. Folic acid conjugation significantly enhanced internalization in SK-BR-3 cells, confirming receptor-mediated endocytosis and supporting their potential for targeted imaging and drug delivery. Overall, grape seed flour–derived N-CDs combine sustainable synthesis, strong optical performance, biocompatibility, and tunable surface chemistry, positioning them as promising nanoplatforms for future breast cancer theranostics. Further studies may explore their use in drug loading and *in vivo* imaging to fully realize their translational potential.

## Conflicts of interest

The authors declare no competing interests.

## Data availability

The data supporting the findings of this study are available within the article. Additional data are available from the corresponding author upon reasonable request.

## Acknowledgements

This work was supported by institutional research facilities and internal resources of the authors' affiliated institutions. No external funding was received.

## References

1 A. A. Madhavan, D. Kushwaha, D. Nath, R. G. Moulick and J. Bhattacharya, Natural occurrence of carbon dots during in vitro nonenzymatic glycosylation of hemoglobin A0, *ACS Omega*, 2022, **7**, 3881–3888.
2 T. D. D. Assuncao, A. Broussier, J. Plain and J. Proust, Unveiling the photoluminescence of carbon quantum dots with controlled cyan or green emission: synthesis and photophysics investigation, *ACS Appl. Opt. Mater.*, 2024, **2**, 1947–1954.
3 X. Li, R. Huang, P. Li, F. K. Tang, J. He, H. Sun and X. Yu, Berberine-Functionalized Bismuth-Doped Carbon Dots in a Pathogen-Responsive Hydrogel System: A Multifaceted Approach to Combating Periodontal Diseases, *ACS Nano*, 2025, **19**, 17554–17577.
4 T. Zhong, Y. Yang, M. Pang, Y. Pan, S. Jing, Y. Qi and Y. Huang, Human serum albumin-coated 10B enriched carbon dots for boron neutron capture therapy, *Adv. Sci.*, 2024, **11**, 202406577.
5 H. Lin, L. Ding, B. Zhang and J. Huang, Detection of nitrite based on fluorescent carbon dots by the hydrothermal method with folic acid, *R. Soc. Open Sci.*, 2018, **5**, 172149.
6 X. Niu, R. Hou, L. Zhang, H. Gao and J. Hu, Synthesis of Multicolor Carbon Dots Catalyzed by Inorganic Salts with Tunable Nonlinear Optical Properties, *Materials*, 2023, **17**, 42.
7 F. Mancini, A. Menichetti, L. D. Esposti, M. Montesi, S. Panseri, G. Bassi and M. Iafisco, Fluorescent Carbon Dots from Food Industry By-Products for Cell Imaging, *J. Funct. Biomater.*, 2023, **14**, 90.

8 A. Sangjan, S. Boonsith, K. Sansanaphongpricha, T. Thinbanmai, S. Ratchahat, N. Laosiripojana and C. Sakdaronnarong, Facile preparation of aqueous-soluble fluorescent polyethylene glycol functionalized carbon dots from palm waste by one-pot hydrothermal carbonization for colon cancer nanotheranostics, *Sci. Rep.*, 2022, **12**, 14704.
9 O. Soledad-Flores, S. J. Bailón-Ruiz and F. R. Román, Rapid Synthesis of Non-Toxic, Water-Stable Carbon Dots Using Microwave Irradiation, *Micro*, 2024, **4**, 659–669.
10 X. Liu, C. Liu, Q. Hu, H. Ge, J. Tan, J. Wang and W. Bian, Dual-response fluorescent carbon dots for Ag+ and Hg2+ detection study in actual samples and biological systems, *Anal. Methods*, 2025, **17**, 6387–6396.
11 Y. Han, W. Li, J. Lin, H. Zhao, X. Wang and Y. Zhang, Carbon quantum dots capped with metal ions for efficient optoelectronic applications, *J. Mater. Chem. C*, 2024, **12**, 5818–5825.
12 A. Selva Sharma and N. Y. Lee, Comprehensive review on fluorescent carbon dots and their applications in nucleic acid detection, nucleolus targeted imaging and gene delivery, *Analyst*, 2024, **149**, 4095–4115.
13 I. Chouzende, A. I. Costa, P. D. Barata, S. Martins, M. C. Semedo, F. M. H. Cardoso and J. V. Prata, Carbon Dots from Porphyridium cruentum Microalgae by High-Efficient Hydrothermal Approaches: Biocompatibility and Antioxidant Capabilities, *ECSOC*, 2023, **27**, 16074.
14 S. Sahana, A. Gautam, R. Singh and S. Chandel, A recent update on development, synthesis methods, properties and application of natural products derived carbon dots, *Nat. Prod. Bioprospect.*, 2023, **13**, 1.
15 L. Wang and H. Zhou, Green Synthesis of Luminescent Nitrogen-Doped Carbon Dots from Milk and Its Imaging Application, *Anal. Chem.*, 2014, **86**, 8902–8905.
16 J. Li, O. Xu and X. Zhu, A facile green and one-pot synthesis of grape seed-derived carbon quantum dots as a fluorescence probe for Cu(ii) and ascorbic acid, *RSC Adv.*, 2021, **11**, 34107–34116.
17 D. Krasteva, Y. Ivanov, Z. Chengolova and T. Godjevargova, Antimicrobial Potential, Antioxidant Activity, and Phenolic Content of Grape Seed Extracts from Four Grape Varieties, *Microorganisms*, 2023, **11**, 395.
18 S. Ragheb, H. E. Wakeel, M. E. Kady, M. M. Moustafa and A. Nofal, A Retrospective Analysis Of Clinicopathological Data And Outcomes Of Hormonal Positive Her2 Negative Metastatic Breast Cancer Patients In Clinical Oncology Department In Ain Shams University Hospitals In Egypt, *Ain Shams Med. J.*, 2022, **73**, 65–75.
19 D. B. Tukaramrao, S. Malla, S. Saraiya, R. A. Hanely, A. Ray, S. Kumari and A. K. Tiwari, A Novel Thienopyrimidine Analog, TPH104, Mediates Immunogenic Cell Death in Triple-Negative Breast Cancer Cells, *Cancers*, 2021, **13**, 1954.
20 C. Capellen, J. Ortega-Rodas, M. J. Morwitzer, H. M. N. Tofilau, M. Dunworth, R. A. Casero and S. Chandra, Hyperglycemic conditions proliferate triple negative breast cancer cells: role of ornithine decarboxylase, *Breast Cancer Res. Treat.*, 2021, **190**, 255–264.
21 S. Mamoor, A single nucleotide variant on chromosome 15 residing within SEMA6D distinguishes patients with basal-like human breast cancer, *OSF Preprints*, 2022, k5sg9.
22 Y. Yao, Y. Zhou, L. Liu, Y. Xu, Q. Chen, Y. Wang and A. Shao, Nanoparticle-based drug delivery in cancer therapy, *Front. Mol. Biosci.*, 2020, **7**, 193.
23 S. Jahan, M. E. Karim and E. H. Chowdhury, Nanoparticle-Based Drug Delivery in Cancer Therapy and Its Role in Overcoming Drug Resistance, *Biomedicines*, 2021, **9**, 114.
24 V. Parvathaneni, S. K. Shukla and V. Gupta, Development and Characterization of Folic Acid-Conjugated Amodiaquine-Loaded Nanoparticles–Efficacy in Cancer Treatment, *Pharmaceutics*, 2023, **15**, 1001.
25 E. Rashidi, N. Esfandiari, Z. Ranjbar, N. Alvandi and Z. Fatahi, Designing of a pH-activatable carbon dots as a luminescent nanoprobe for recognizing folate receptor-positive cancer cells, *Nanotechnology*, 2021, **33**, 075103.
26 Y. Tang, Q. Xu, X. Zhang, *et al.*, Expediting carbon dots synthesis by the active adaptive method with machine learning and applications in dental diagnosis and treatment, *Nano Res.*, 2024, **17**, 10109–10118.
27 B. D. Karuppasamy, S. Perumal, R. Atchudan, A. K. Sundramoorthy, S. Ramalingam, D. Manoj, S. Sangaraju, T. N. J. I. Edison, S. W. Lee and Y. R. Lee, Hydrothermal synthesis of intrinsic carbon dots with tunable emission for fluorescent inks and variegated bioimaging applications, *J. Mol. Liq.*, 2025, **437**, 128592, DOI: 10.1016/j.molliq.2025.128592.
28 B. D. Karuppasamy, S. Perumal, R. Atchudan, A. K. Sundramoorthy, S. Ramalingam, D. Manoj, R. S. Babu, J. H. Park and S. W. Lee, Cornus Officinalis-derived hydrophilic carbon dots with regulatable emission for in-vivo imaging with good biocompatibility, *Inorg. Chem. Commun.*, 2025, **182**, 115350, DOI: 10.1016/j.inoche.2025.115350.
29 K. Dev, S. Singh, S. Bhardwaj, S. Samanta, R. Saroha, P. Roy, K. Ghosh and P. K. Maji, Green synthesis of biomass-derived nitrogen-doped carbon dots for selective Co2+ and nitric oxide sensing and bioimaging applications, *Langmuir*, 2025, **41**, 16843–16856, DOI: 10.1021/acs.langmuir.5c00961.
30 M. Y. Pudza, Z. Z. Abidin, S. A. Rashid, F. M. Yassin, A. S. M. Noor and M. Issa, Synthesis and Characterization of Fluorescent Carbon Dots from Tapioca, *ChemistrySelect*, 2019, **4**, 4140–4146.
31 Z. Peng, Y. Zhou, C. Ji, J. Pardo, K. J. Mintz, R. R. Pandey and R. M. Leblanc, Facile Synthesis of "Boron-Doped" Carbon Dots and Their Application in Visible-Light-Driven Photocatalytic Degradation of Organic Dyes, *Nanomaterials*, 2020, **10**, 1560.
32 K. Phetcharee, T. Jorn-am, W. Pholauyphon, T. Kwamman, N. Sirisit, J. Manyam and P. Paoprasert, The Fabrication of Amine-Incorporated Zinc Complex/Carbon Dot Composite Electrodes Using Gamma Irradiation for High-Performance Supercapacitors, *ChemistrySelect*, 2023, **8**, e202301428.
33 G. Gedda, S. A. Sankaranarayanan and C. L. Putta, Green synthesis of multi-functional carbon dots from medicinal

plant leaves for antimicrobial, antioxidant, and bioimaging applications, *Sci. Rep.*, 2023, **13**, 6371.
34 J. Schneider, C. J. Reckmeier, Y. Xiong, M. von Seckendorff, A. S. Susha, P. Kasák and A. L. Rogach, Molecular Fluorescence in Citric Acid-Based Carbon Dots, *J. Phys. Chem. C*, 2017, **121**, 2014–2022.
35 D. Zhao, W. Ma, R. Wang, X. Yang, J. Li, T. Qiu and X. Xiao, The Preparation of Green Fluorescence-Emissioned Carbon Dots/Poly(N-Isopropylacrylamide) Temperature-Sensitive Hydrogels and Research on Their Properties, *Polymers*, 2019, **11**, 1171.
36 M. Cutroneo, L. Silipigni, P. Malínský, P. Slepička, D. Franco and L. Torrisi, Polyvinylalcohol Composite Filled with Carbon Dots Produced by Laser Ablation in Liquids, *Polymers*, 2024, **16**, 1390.
37 T. Bhattacharya, S. Preetam and S. Mukherjee, Anticancer activity of quantum size carbon dots: opportunities and challenges, *Discover Nano*, 2024, **19**, 122.
38 A. Coroaba, M. Ignat and O. E. Carp, Antioxidant activity and in vitro fluorescence imaging application of N-, O-functionalized carbon dots, *Sci. Rep.*, 2025, **15**, 25834.
39 I. Isnaeni, V. Purwandari, P. A. Putro and H. M. Adiwidya, Optical Properties of Sodium-doped Carbon Dots Made of Urea and Trisodium Citrate, *TIME Phys.*, 2023, **1**, 1–9.
40 K. J. Mintz, M. Bartoli, M. Rovere, Y. Zhou, S. D. Hettiarachchi, S. Paudyal and R. M. Leblanc, A deep investigation into the structure of carbon dots, *Carbon*, 2021, **173**, 433–447.
41 A. Pal, M. P. Sk and A. Chattopadhyay, Recent advances in crystalline carbon dots for superior applications, *Mater. Adv.*, 2020, **1**, 525–553.
42 N. Kaushal, A. Jain, A. Kumar, S. Sarraf, A. K. Basu, C. I. Raje and A. Saha, Solvent-Free Synthesis of S,N-Doped Carbon Dots for Extended Visible-Light-Induced Oxidase-Mimicking Activities and Antimicrobial Applications, *ChemPlusChem*, 2023, **88**, e202300125.
43 P. Xiao, L. Zhao, Z. Sui and B. Han, Synthesis of Core–Shell Structured Porous Nitrogen-Doped Carbon@Silica Material via a Sol–Gel Method, *Langmuir*, 2017, **33**, 6038–6045.
44 P. Su, Q. Jiao, H. Li, Y. Li, X. Liu, Q. Wu and W. Wang, Rational Design of $NiCo_2S_4$ Quantum Dot-Modified Nitrogen-Doped Carbon Nanotube Composites as Robust Pt-Free Electrocatalysts for Dye-Sensitized Solar Cells, *ACS Appl. Energy Mater.*, 2021, **4**, 4344–4354.
45 K. Artyushkova, A. Serov, S. Rojas-Carbonell and P. Atanassov, Chemistry of Multitudinous Active Sites for Oxygen Reduction Reaction in Transition Metal–Nitrogen–Carbon Electrocatalysts, *J. Phys. Chem. C*, 2015, **119**, 25917–25928.
46 V. Arul and M. G. Sethuraman, Hydrothermally Green Synthesized Nitrogen-Doped Carbon Dots from Phyllanthus emblica and Their Catalytic Ability in the Detoxification of Textile Effluents, *ACS Omega*, 2019, **4**, 3449–3457.
47 A. G. Roy, J. M. Robinson, P. Sharma, A. Rodriguez-Garcia, M. A. Poussin, C. Nickerson-Nutter and D. J. Powell Jr, Folate Receptor Beta as a Direct and Indirect Target for Antibody-Based Cancer Immunotherapy, *Int. J. Mol. Sci.*, 2021, **22**, 5572.
48 T. Gonzalez, M. Muminovic, O. Nano and M. Vulfovich, Folate Receptor Alpha—A Novel Approach to Cancer Therapy, *Int. J. Mol. Sci.*, 2024, **25**, 1046.
49 A. Angelopoulou, A. Kolokithas-Ntoukas, C. Fytas, K. Avgoustakis and F. Acid-Functionalized, Condensed Magnetic Nanoparticles for Targeted Delivery of Doxorubicin to Tumor Cancer Cells Overexpressing the Folate Receptor, *ACS Omega*, 2019, **4**, 22214–22227.
50 A. M. Fales, B. M. Crawford and T. Vo-Dinh, Folate Receptor-Targeted Theranostic Nanoconstruct for Surface-Enhanced Raman Scattering Imaging and Photodynamic Therapy, *ACS Omega*, 2016, **1**, 730–735.
51 Y. Zheng, G. Xie, X. Zhang, Z. Chen, Y. Cai, W. Yu, H. Liu, J. Shan, R. Li, Y. Liu and B. Lei, Bioimaging Application and Growth-Promoting Behavior of Carbon Dots from Pollen on Hydroponically Cultivated Rome Lettuce, *ACS Omega*, 2017, **2**, 3958–3965, DOI: 10.1021/acsomega.7b00657.